Supporting Information

Photoactivated Defect Engineering and Nanostructure Functionalization of MoS_2 via a Photochemical Fenton Process

Tuan-Hoang Tran[a], Raul D. Rodriguez[a]*, Aura Garcia[a], Qiang Ma[b], Tao Zhang[b], Ranran Wang[c], Evgeniya Sheremet[a]

[a]Tomsk Polytechnic University, Lenina avenue, 30, 634050, Tomsk, Russia

[b]Key Laboratory of Marine Materials and Related Technologies, Ningbo Institute of Materials Technology and Engineering, Chinese Academy of Sciences, Ningbo 315201, China

[c]Shanghai Institute of Ceramics, Chinese Academy of Sciences, Shanghai, China

*Corresponding author. E-mail: raul@tpu.ru

Table S1. Comparison of MoS_2 production methods[1,2]

Methods	Advantages	Disadvantages
Mechanical exfoliation	High-quality and large-area flakes	Low yield, low reproducibility, low defect density
Chemical vapor deposition	Large-area monolayers, scalability	Low yield, poor layer thickness control, high temperature synthesis, low-defect density
Chemical liquid exfoliation	Mass production under ambient conditions, high-defect density	Non-uniform thickness, Aggressive chemical agents, small flake area
Wet chemical synthesis	Controllability of surface morphology, crystallite size and dopant	High pressure, aggressive chemical agents,

	mass production, high-defect density	non-uniform thickness
Plasma-assisted thinning	Large flake area, controlled thickness, high-defect density	Instrument dependency, high production cost, limited yield
Our method	Large flake area, scalability, environmentally-friendly chemical agents, rapid etching, high defect density	Non-uniform thickness

Table S2. pH of MoS_2 dispersion, $FeCl_3$ and MoS_2+$FeCl_3$ solution with and without illumination for 2 hours

Solution	**0.05 M MoS_2**	**0.05 M $FeCl_3$**	**0.05 M MoS_2/ 0.05 M $FeCl_3$**
In dark for 2 hours	6.5	6.0	5.75
Under illumination for 2 hours	6.25	5.5	5.5

The pH of MoS_2 solution in dark and under illumination are 6.5 and 6.25, respectively. The decrease in pH - 0.25 due to the oxidation of MoS_2 according to following reaction:

$$MoS_2 + 18\bullet OH \rightarrow MoO_4^{2-} + 2SO_4^{2-} + 6H_2O + 6H^+$$

The pH of $FeCl_3$ solution in dark and under illumination are 6.0 and 5.5, respectively. The decrease in pH - 0.5 may result from the acceleration of reaction:

$$Fe^{3+} + H_2O \rightarrow Fe(OH)_2^+ + H^+$$

The pH of MoS_2+$FeCl_3$ solution in dark and under illumination are 5.75 and 5.5, respectively. The decrease in pH of MoS_2+$FeCl_3$ solution after illumination is 0.25, which is than the sum of pH decrease in MoS_2 dispersion alone (0.25) and $FeCl_3$ solution alone (0.5) after illumination. This can be explained by the generation of OH^- in Fenton-reaction, which compensates H+ and reduces the overall decrease in pH:

$$Fe^{2+} + H_2O_2 \rightarrow Fe^{3+} + OH^- + \bullet OH$$

Electron paramagnetic resonance (EPR) spectroscopy experiment

To further elucidate the role of reactive oxygen species (ROS) in the photo-driven Fenton process and validate the proposed mechanism, we conducted electron paramagnetic resonance

(EPR) spectroscopy experiments to detect hydroxyl (•OH) radicals directly, a key species in the oxidation or etching of MoS_2.

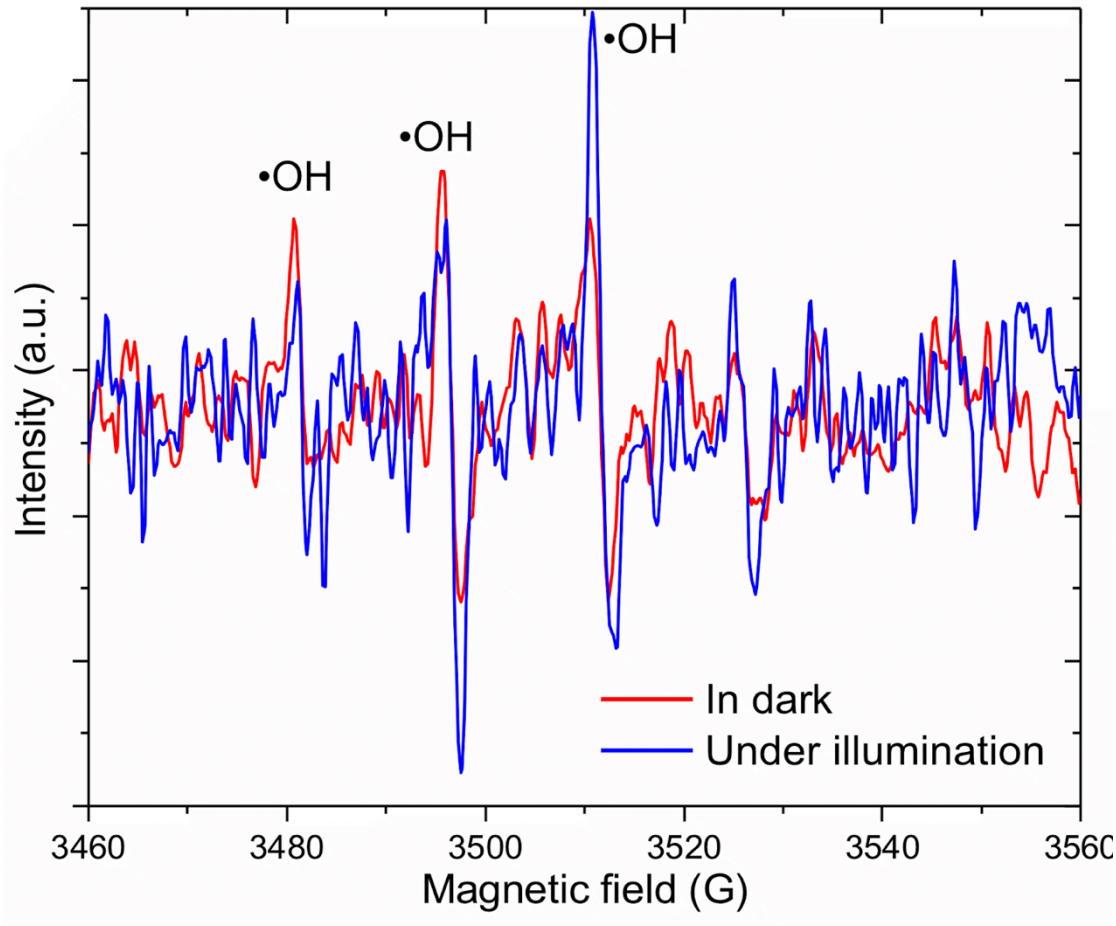

Figure S1 EPR spectra of DMPO-radical adducts in MoS_2+$FeCl_3$ in dark and under illumination

In the dark, the presence of •OH radicals was detected in the sample containing MoS_2 and $FeCl_3$ with 3,4-dihydro-2,3-dimethyl-2H-pyrrole 1-oxide (DMPO), indicating baseline ROS generation from MoS_2 oxidation in water[3]. Under Xenon lamp illumination, the •OH signal increased, confirming the photo-driven nature of the Fenton reaction (see Figure S1). In both cases of MoS_2+$FeCl_3$ without and with illumination, the signal-to-noise ratio of •OH radicals is low, which is explained by the conversion of paramagnetic DMPO-OH to diamagnetic intermediates in high Fe^{3+} concentration solution under acidic conditions[4]. Hence, it is unreliable to quantify the amount of •OH radicals based on EPR spectra because it underestimates the amount of DMPO-OH radicals, part of which is converted to diamagnetic form and not registered in the EPR spectra. Despite this, the EPR spectra can still give a qualitative conclusion; detecting of •OH in both dark and illuminated conditions supports its role in the etching mechanism. The enhanced •OH signal under illumination aligns with our proposed mechanism, where photogenerated charge carriers in MoS_2 reduce Fe^{3+} to Fe^{2+} and produce H_2O_2, which reacts to form •OH radicals, oxidizing MoS_2 and generating metal-based nanostructures at the reaction sites.

Superoxide ($\bullet O_2^-$) radicals were not detected, likely due to their short lifetime, rapid conversion into H_2O_2 or participation in the Haber-Weiss reaction ($\bullet O_2^- + H_2O_2 \rightarrow$ ***(Fe^{2+}/Fe^{3+})*** $+ O_2 + HO^- + HO\bullet$)[5], their absence in EPR does not invalidate the mechanism but reflects the dynamic ROS interplay.

This EPR data confirms the presence of •OH radicals generated via a photo-driven Fenton reaction, thus validating the proposed mechanism for photoactivated defect engineering and nanostructure functionalization of MoS_2 in $FeCl_3$ solution under illumination.

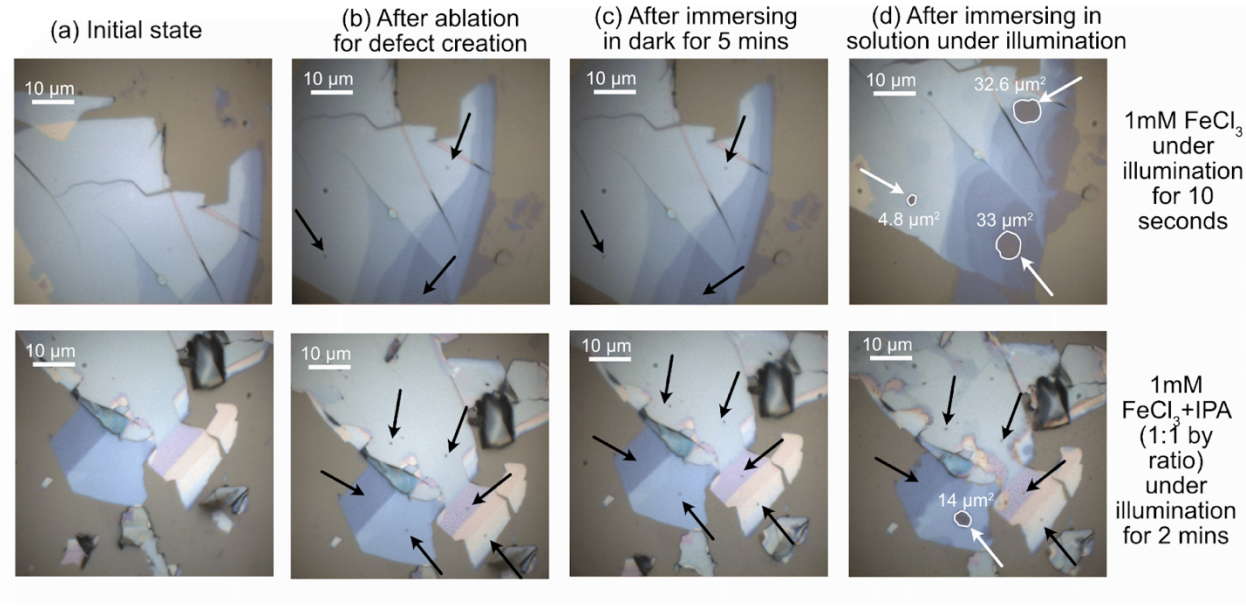

Figure S2 •OH quenching experiment with isopropyl alcohol (IPA): Optical images of (a) MoS_2 initial state, (b) after ablation for defect creation, (c) after immersing in solution in dark for 5 minutes, (d) after immersing in solution under halogen lamp illumination. First row: 1 mM $FeCl_3$ solution under illumination for 10 seconds; Second row: 1 mM $FeCl_3$+ IPA (1:1 by volume ratio) for 2 minutes. The etching rate is smaller in the case of $FeCl_3$ +IPA

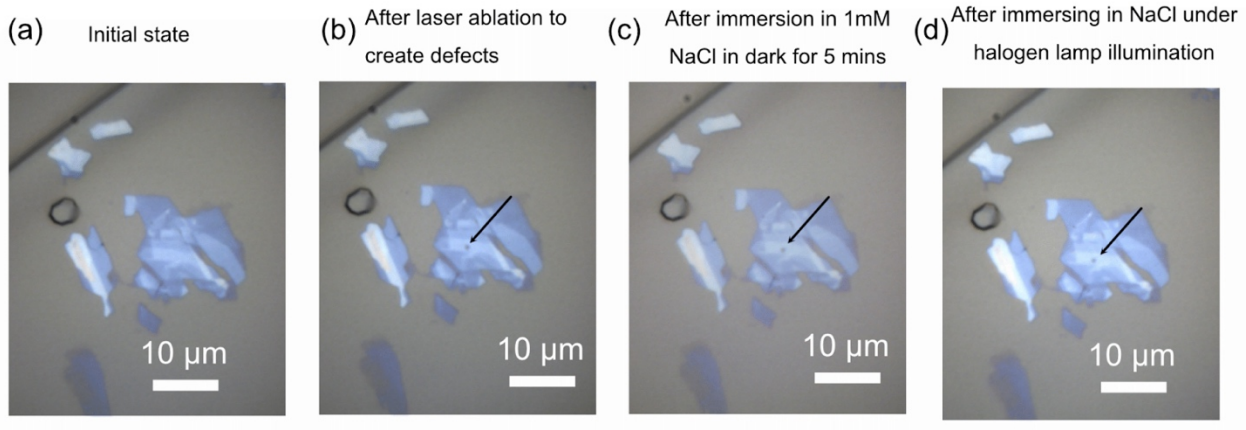

Figure S3 Optical image of MoS_2 on HOPG in NaCl solution (a) initial flake, (b) after laser ablation to create defects , (c) after immersion in solution in dark for 5 mins, proving no spontaneous reaction between MoS_2 and NaCl, (d) after illumination by the halogen lamp at the power of 22.5 mW for 5 mins with 100x objective in NaCl solution. The black arrows show the laser-carved spots. No changes in the optical image were observed.

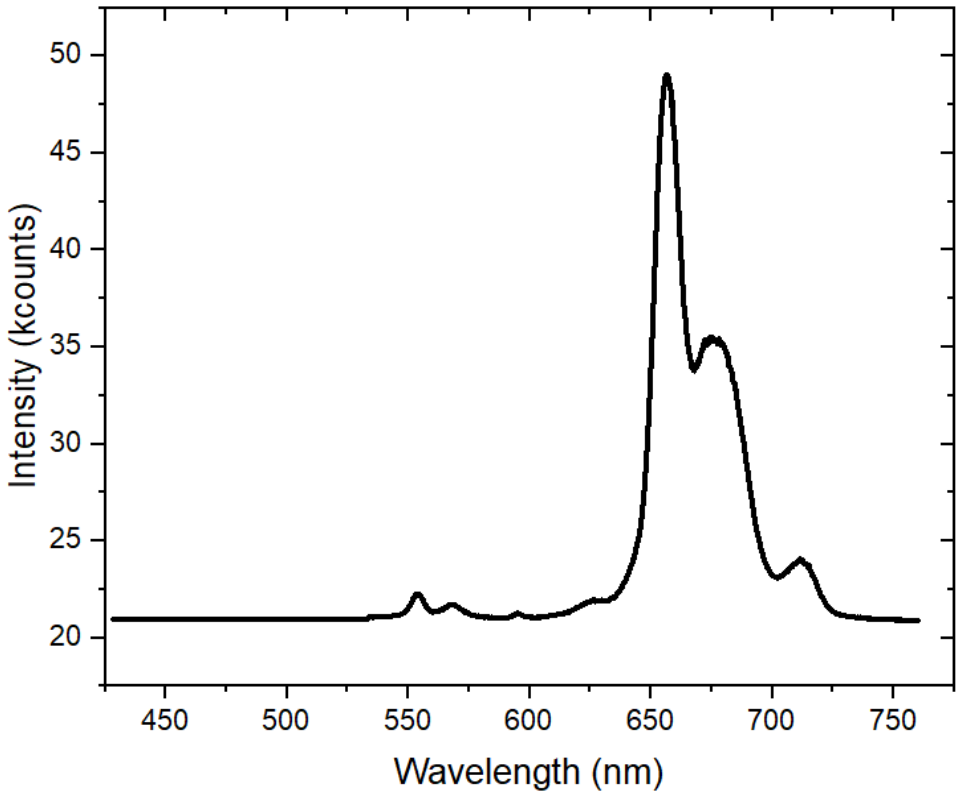

Figure S4. Spectrum of halogen lamp, employed in the experiment

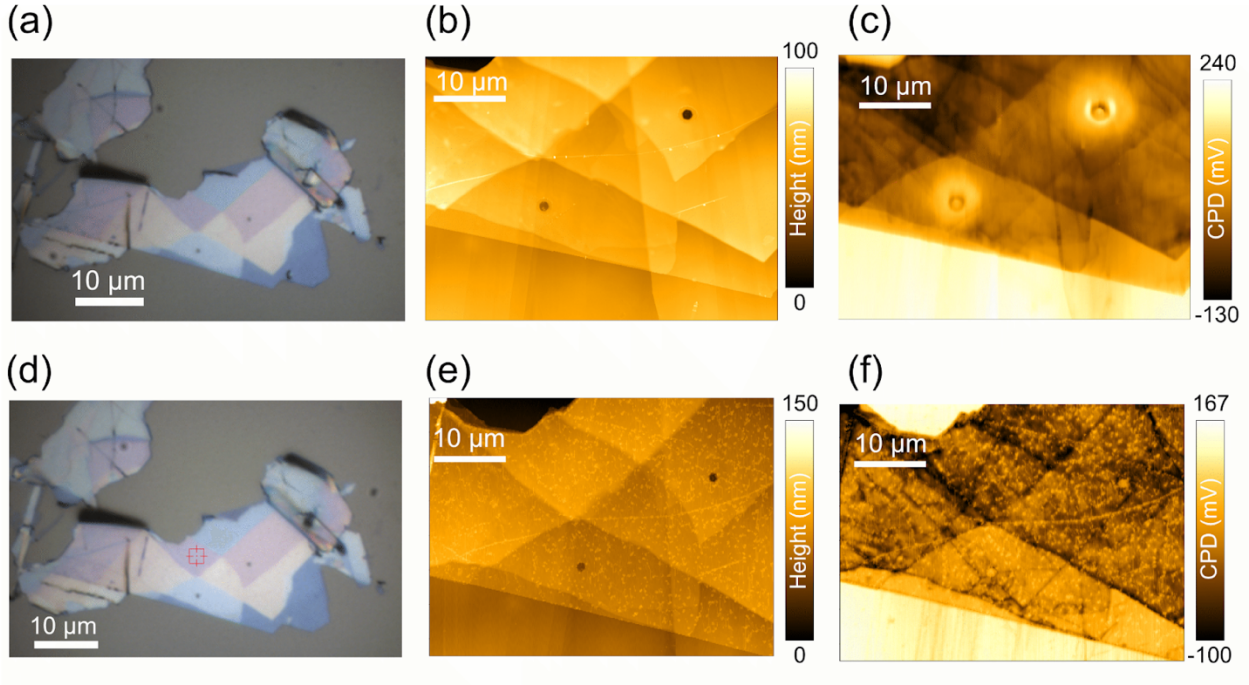

Figure S5. (a) Optical image, (b) AFM image, (c) KPFM image of MoS_2 on HOPG before immersing in $FeCl_3$ solutions; (d) Optical image, (e) AFM image, (f) KPFM image of MoS_2 on HOPG after immersing in $FeCl_3$ solution in dark condition for 5 mins.

The change in work function at the laser-carved spots in Figure S5 may result from the deposition of iron oxide on MoS_2. This iron oxide forms on both MoS_2 and HOPG due to the oxidation of Fe^{3+} by dissolved oxygen in water because Fe^{3+} is a good oxygen scavenger.

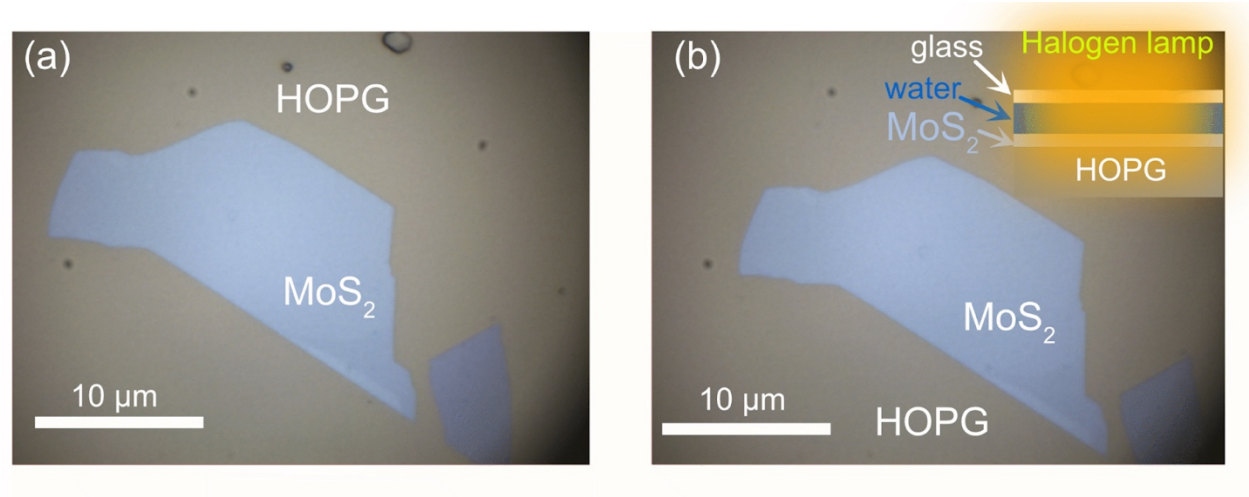

Figure S6. Multilayer MoS_2 flake on HOPG (a) initial flake, (b) after illumination in water for 5 minutes by halogen lamp (inset: the experiment schematic)

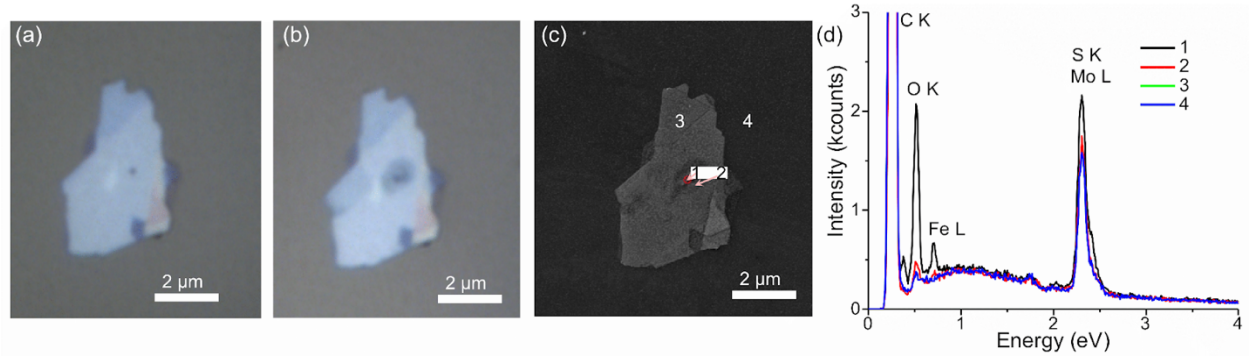

Figure S7 Optical image of MoS_2 flake (a) before and (b) after illumination in $FeCl_3$ solution by halogen lamp, (c) SEM image of MoS_2 after illumination in $FeCl_3$ solution, (d) the EDX spectra at 4 points marked in (c)

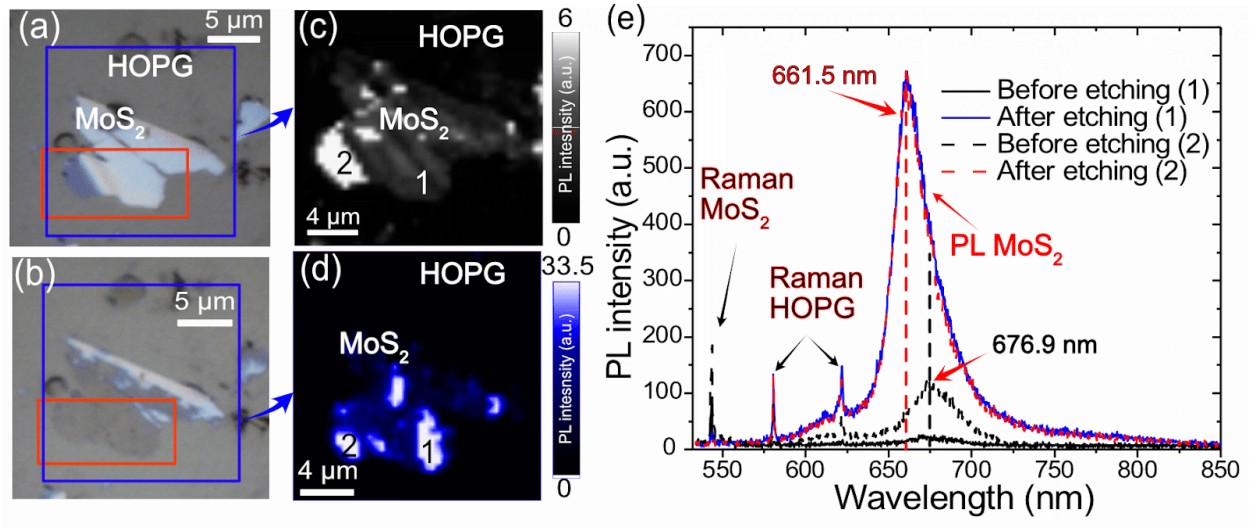

Figure S8. Optical image of MoS_2 flakes (a) prior and (b) following photoetching; PL map of MoS_2 peak (c) before and (d) after photoetching process (the blue rectangular in Figure S4(a) and (b), respectively); (f) PL spectra of MoS_2 at point (1) and (2) in Figure S4(c) and 1(d).

The observed blue shift in PL from 676.9 nm to 661.5 nm at point (2) could be associated to the defect formation or doping that occurs during the etching process (The fitting in PL spectra is in Figure S8).[6,7]

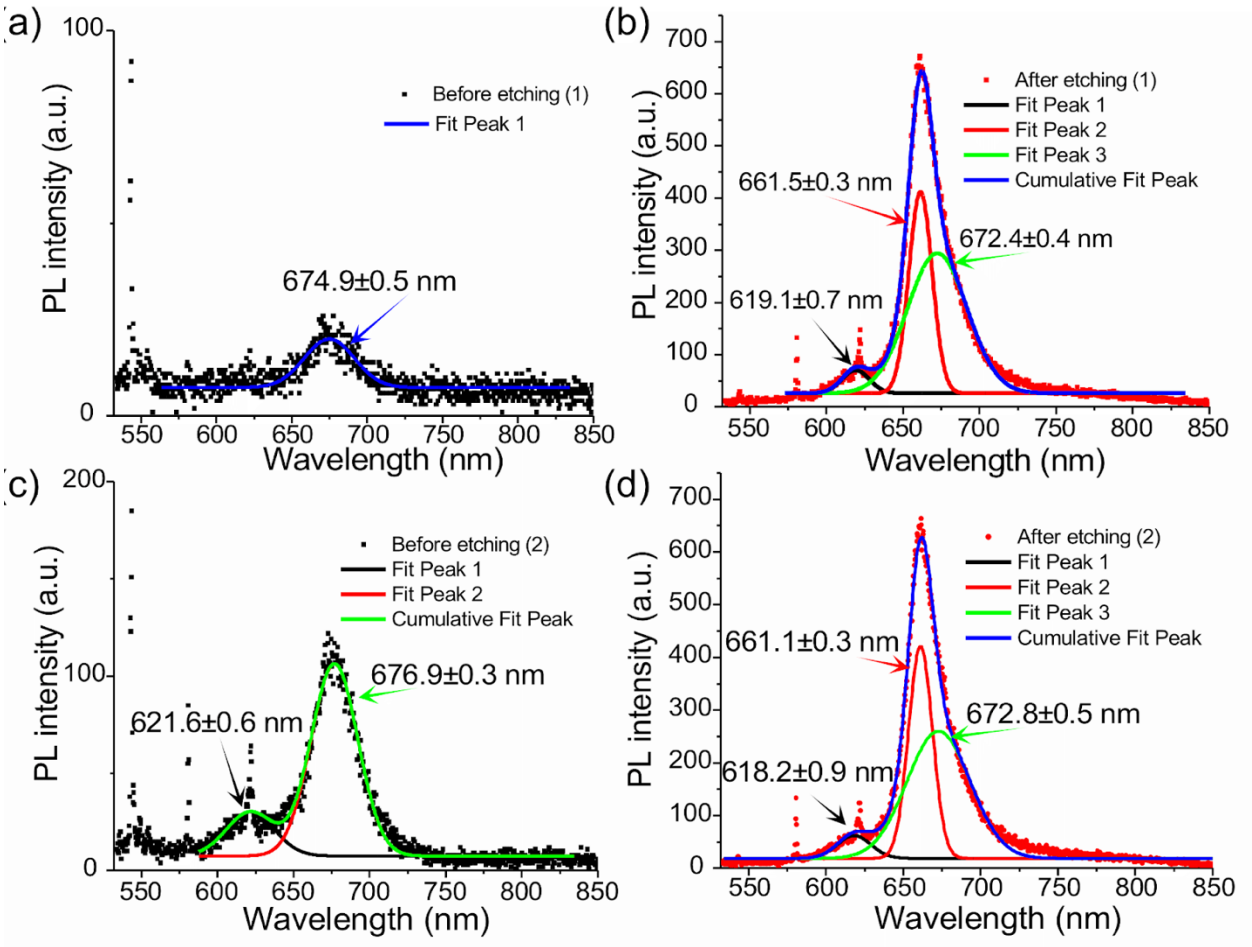

Figure S9. The fitting of photoluminescence (PL) spectra (a) before and (b) after etching at point (1); (c) before and (d) after etching at point (2)

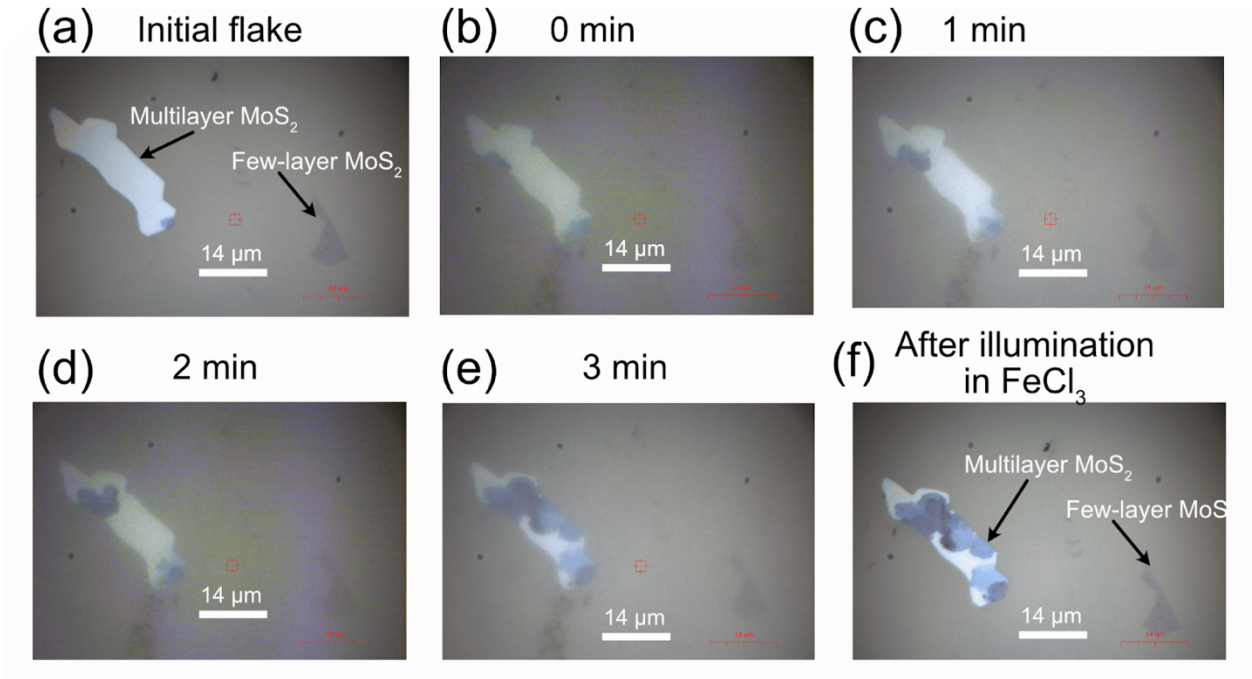

Figure S10. Optical image of multilayer and few-layer MoS_2 flakes (a) initial flakes, taken in air, optical images of multilayer and few-layer MoS2 flakes, taken while illuminating in $FeCl_3$ solution by halogen lamp at (b) 0 min, (c) 1 min, (d) 2 min, (e) 3 min, (f) after illumination in $FeCl_3$ solution, taken in air

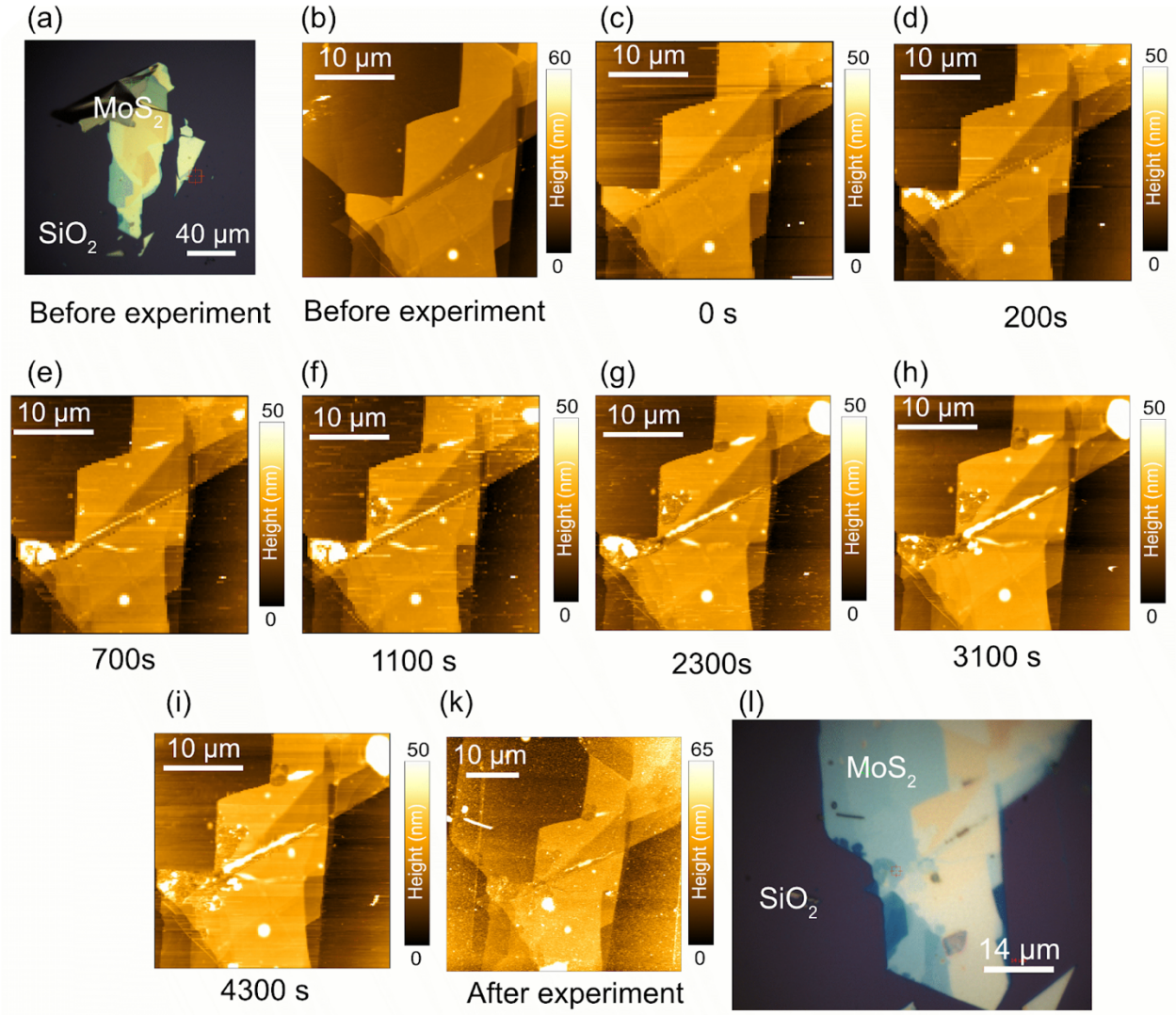

Figure S11 (a) Optical image and (b) AFM image of MoS_2 on SiO_2/Si before experiment in $FeCl_3$. AFM images of MoS_2 on SiO_2/Si in $FeCl_3$ at different starting time of AFM scans: (c) 0 s, (d) 200 s, (e) 700 s, (f) 1100 s, (g) 2300 s, (h) 3100 s, (i) 4300 s. (k) AFM image and (l) optical image of MoS_2 on SiO_2/Si after experiment in $FeCl_3$. We can clearly see the change in topography, indicating the etching of MoS_2

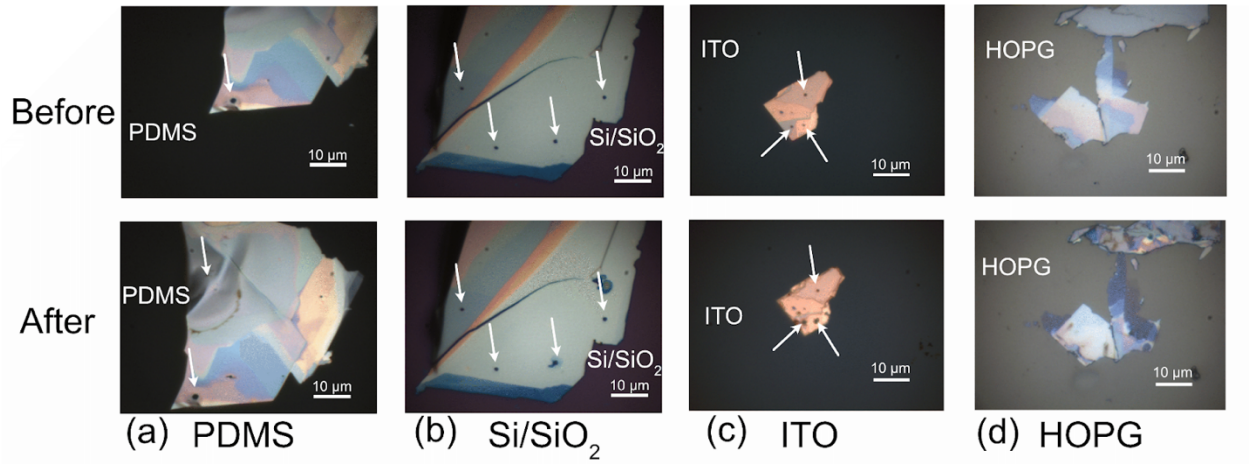

Figure S12 Optical image of MoS2 on different substrate: (a) polydimethylsiloxane (PDMS), (b) Si/SiO_2, c) tin-indium oxide (ITO), d) highly-oriented pyrolytic graphite (HOPG) before and after illumination by halogen lamp in 1 mM $FeCl_3$ (the arrows shows the laser-carved spots).

The effect of substrate on photoetching of MoS_2 in $FeCl_3$ solution was investigated. Four popular substrates: polydimethylsiloxane (PDMS), Si/SiO_2, tin-indium oxide (ITO), and highly-oriented pyrolytic graphite (HOPG) were selected. The photoetching is most effective for MoS_2 on HOPG. No etching was observed for MoS_2 on PDMS.

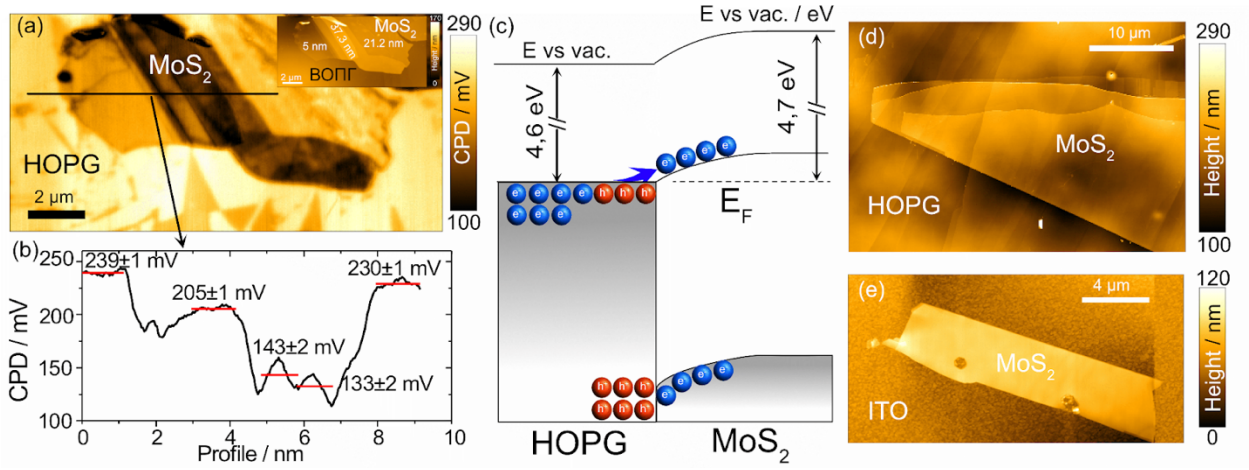

Figure S13. (a) Kelvin probe force microscopy (KPFM) image of MoS_2 on HOPG, (b) contact potential difference (CPD) profile of MoS_2 on HOPG in Figure S13a, (c) band diagram of MoS_2 and HOPG.

As proposed in the photoetching mechanism, the free-charge concentration is needed for effective photoetching. The free-charge concentration of MoS2 can be affected by the charge concentration of the substrate. To investigate the effect of conductive substrate on charge concentration of MoS_2, we conducted Kelvin probe force microscopy (KPFM) measurement. The results are presented in Figure S13. The Figure S13(a) shows the KPFM image of multilayer MoS_2 on HOPG. The triangle domain of contact potential difference (CPD) on HOPG in KPFM image is related to twisted bilayer graphene on HOPG[8]. The MoS_2's CPD is clearly smaller than HOPG's value. HOPG shows a CPD of 239 ± 1 mV, while MoS_2 exhibits a CPD of 205 ±1 mV at 5 nm thickness and 133 ± 2 mV at 37.3 nm thickness (see the profile in Figure S13(b)). Using HOPG's

standard reference work function of 4.6 eV[9], we calculated MoS_2 work functions of 4.64 ± 0.01 eV (5 nm) and 4.70 ± 0.01 eV (37.3 nm). The rise in the work function of MoS_2 work function increases with the layer thickness due to the electrostatic screening in MoS_2[10,11].

Since the MoS_2 work function is larger than that of HOPG, electrons move from HOPG to MoS_2 upon contact to align Fermi levels without encountering Schottky barrier.[12] This electron transfer creates downward banding in MoS_2 at the MoS_2/HOPG interface (see Figure S13(c), increasing the electron concentration at MoS_2/HOPG interface. Consequently, etching occurs preferentially at the MoS_2/HOPG/water interface rather than basal plane MoS_2/water interface (see Figure S10). Hence, the photoetching of MoS_2 on conductive ITO and HOPG substrates is more effective than on non-conductive substrates PDMS and Si/SiO_2.The remarkable charge transfer between MoS_2 and graphene layers on HOPG[13,14] compared to other metal substrates increases the charge concentrations in MoS_2, leading to the most effective photoetching of MoS_2 in $FeCl_3$ solution.

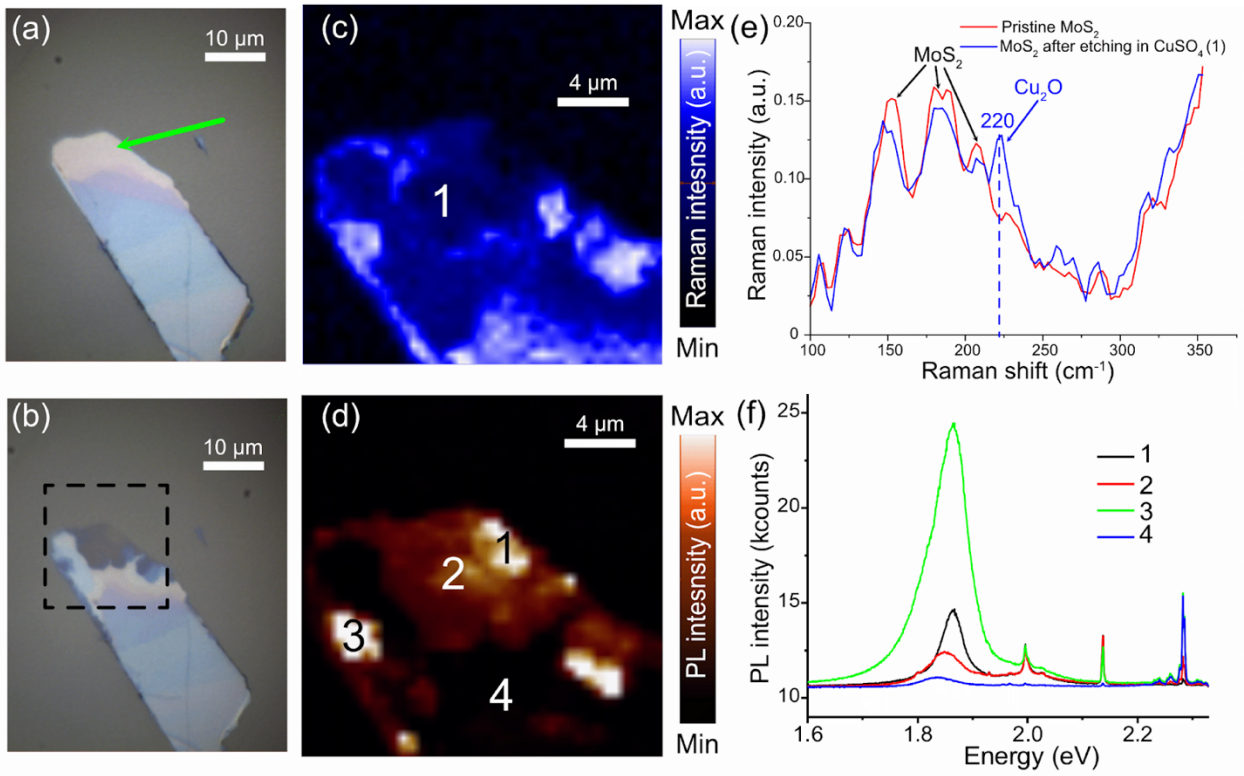

Figure S14 Optical images of MoS_2 (a) before and (b) after photoetching in 1 M $CuSO_4$ solution by laser irradiation of 532 nm laser with the power of 0.1 mW through 100x objective (an arrow shows the laser irradiation spot). (c) Raman and (d) photoluminescence (PL) intensity map of MoS_2 after photoetching in $CuSO_4$ (scan area within the black dashed line in Figure S14(b)). (e) Raman spectra of pristine and photoetched MoS_2 in $CuSO_4$ at point (1) in Figure S14(c), identifying Cu_2O peak at 220 cm^{-1}. (f) PL spectra at points 1–4 in Figure S14(d), showing enhanced PL intensity after photoetching, indicating a successful etching from multilayer to few-layer MoS_2.

After irradiating MoS_2 in $CuSO_4$ with a 532 nm laser, we observed changes in optical images, indicating successful MoS_2etching (see Figure S14(a)-(b)). The decrease in Raman intensity and

increase in photoluminescence (PL) intensity (Figure S14(c)-(d)) confirms the etching of multilayer to few-layer MoS_2. The Raman spectra after photoetching in $CuSO_4$ (Figure S14(e)) show an additional peak at 220 cm^{-1}, suggesting the presence of Cu_2O[15]. Figure S14(f) demonstrates strong PL enhancement after the etching process, confirming the etching of multilayer to few-layer MoS_2.

1 S. H. Choi, S. J. Yun, Y. S. Won, C. S. Oh, S. M. Kim, K. K. Kim and Y. H. Lee, *Nat. Commun.*, 2022, **13**, 1484.

2 P. Zhang, H. Xiang, L. Tao, H. Dong, Y. Zhou, T. S. Hu, X. Chen, S. Liu, S. Wang and S. Garaj, *Nano Energy*, 2019, **57**, 535–541.

3 D. Ghim, P.-I. Chou, S. H. Chae and Y.-S. Jun, *Environ. Sci. Technol.*, 2021, **55**, 13759–13769.

4 J. M. Fontmorin, R. C. Burgos Castillo, W. Z. Tang and M. Sillanpää, *Water Res.*, 2016, **99**, 24–32.

5 J. P. Kehrer, *Toxicology*, 2000, **149**, 43–50.

6 S. Mouri, Y. Miyauchi and K. Matsuda, *Nano Lett*, 2013, **13**, 5944–5948.

7 P. K. Chow, R. B. Jacobs-Gedrim, J. Gao, T.-M. Lu, B. Yu, H. Terrones and N. Koratkar, *ACS Nano*, 2015, **9**, 1520–1527.

8 T.-H. Tran, R. D. Rodriguez, M. Salerno, A. Matković, C. Teichert and E. Sheremet, *Carbon N. Y.*, 2021, **176**, 431–439.

9 P. A. Fernández Garrillo, B. Grévin, N. Chevalier and Ł. Borowik, *Rev. Sci. Instrum.*, 2018, **89**, 043702.

10 C. Lattyak, K. Gehrke and M. Vehse, *J. Phys. Chem. C Nanomater. Interfaces*, 2022, **126**, 13929–13935.

11 A. Sohn, H. Moon, J. Kim, M. Seo, K.-A. Min, S. W. Lee, S. Yoon, S. Hong and D.-W. Kim, *J. Phys. Chem. C Nanomater. Interfaces*, 2017, **121**, 22517–22522.

12 Z. Zhang and J. T. Yates Jr, *Chem. Rev.*, 2012, **112**, 5520–5551.

13 H. Li, K. Yu, C. Li, Z. Tang, B. Guo, X. Lei, H. Fu and Z. Zhu, *Sci. Rep.*, 2015, **5**, 18730.

14 L. Yu, Y.-H. Lee, X. Ling, E. J. G. Santos, Y. C. Shin, Y. Lin, M. Dubey, E. Kaxiras, J. Kong, H. Wang and T. Palacios, *Nano Lett.*, 2014, **14**, 3055–3063.

15 Y. Deng, A. D. Handoko, Y. Du, S. Xi and B. S. Yeo, *ACS Catal.*, 2016, **6**, 2473–2481.